Highly thermal conductive Boron Nitride/Polyrotaxane encapsulated PEG-based phase change materials

Guang-Zhong Yin, [a, b, *] Xiao-Mei Yang, [b, c] Alba Marta López, [b] Javier García Molleja, [b] Antonio Vázquez-López, [b] De-Yi Wang [a, b, *]

[a] *Escuela Politécnica Superior, Universidad Francisco de Vitoria, Ctra. Pozuelo-Majadahonda Km 1.800, 28223, Pozuelo de Alarcón, Madrid, Spain*

[b] *IMDEA Materials Institute, C/Eric Kandel, 2, 28906 Getafe, Madrid, Spain*

[c] *Fibre and Particle Engineering, P.O. Box 4300, FI-90014, University of Oulu, Oulu, Finland*

Corresponding authors

*Tel: +34 91 549 34 22, Email: deyi.wang@imdea.org

*Tel: +34 61 566 44 38, Email: amos.guangzhong@ufv.es

Abstract. In this work, we tried to overcome the typical limitations of phase change materials (PCMs), namely, leakage and low thermal conductivity. To realize the leakage proof PCM, a polyrotaxane (PLR) was selected as a support material to encapsulate Polyethylene glycol (PEG) 1k. Subsequently, different contents of Boron Nitride (BN) were blended to enhance the thermal conductivity of PLR/PEG matrix. The PCMs created in this work achieves a high thermal performance with enthalpy values (91.2-123.5 J/g) and high flexibility and shows a great shape stability and no leakage and shape change during its phase transition. Due to the action of BN as a multifunctional filler, the PCMs also experienced an increase of 186.7% to 806.7% in thermal conductivity values, and enhanced flame retardancy (with decrease of 16.6% for pHRR and 25.5% for THR). These improvements solve the main problems of organic PCMs thus making PLR-PEG-

BN based materials a good candidate to be used as thermal energy storage material in industrial applications. For the exact application cases, it showed obvious Peak Shaving and Valley Filling for thermoelectric generator and heat regulation for the smart phone.

Keywords: Polyrotaxane; Phase Change Materials; Boron Nitride; Flexible composites; Energy storage

1. INTRODUCTION

With the development of technologies and the implementation of 5G, the thermoregulation of devices has become a problem, since they consume more and more energy and therefore generate more heat that must be dissipated.[1] The use of ecofriendly materials and the development of green energy management materials has become necessary to avoid environmental problems in the future, such as pollution and the depletion of fossil resources and the increase of adverse effects of climate change. [2]

Among the thermal energy storage and thermal regulation materials, the phase change materials (PCM) stand out. These materials can store energy in the form of latent heat and release the energy when there is a difference in environmental temperature, this energy exchange occurs when there is a phase change of the material itself.[3] Within the many applications of PCM are: temperature adaptable greenhouses,[4] solar energy storage, [5]smartphone thermal regulation,[6] solar thermoelectric generator, [7] and so on. The main problems of PCMs in general, from their commercialization and production, are a low thermal conductivity, poor form stability, and PCM work substance leakage during the phase change that cause failures in the process. [8] Another main problem of PCMs is the difficulty of obtaining flexible phase change energy storage materials, because many of the prepared materials are rigid or in powder form, which require secondary processing for practical applications.[9]

Within these organic PCMs, polyethylene glycol (PEG) based PCMs are widely used as energy storage materials in the fields of solar energy uses, [10] waste heat recovery, [11] and electric energy storage.[12] Among the properties of PEG are its large phase transformation enthalpy, wide transition temperature range, thermal and chemical

stability, ease of chemical modification, good biocompatibility, low vapor pressure, and non-toxic nature.[13] But like all organic PCMs, they have the same typical drawbacks, which are low thermal conductivity, and leakage during the phase change from solid to liquid.

To generate form stable PEG based PCM composites, there are three common ways: the first is encapsulation of PEG in shell materials.[14] Another way would be the preparation of polymer/PEG blending composites.[15,16] The third method is the impregnation of PEG into inorganic materials with porous or layered structures, such as Graphene [17], Graphene oxide,[18] MXene, [19] Boron nitride, [20] or other carbon based functional fillers.[21] But these inorganic components mean that the more their content grows, the less flexible the material becomes, in addition to losing energy retention capacity in the form of latent heat.[12] Nevertheless, the developed composite PCMs are usually brittle and possess lower mechanical strength, thus remained unable to meet the flexibility requirements, which is a key property to utilize PCMs for thermal management of advanced electronic devices, the human body, and many other applications. Therefore, it is highly desired to develop PCMs that possess the flexibility to be explored for widespread application. [22]

In the previous report, the Polyrotaxane (PLR) was prepared with a simple and green pathway.[9] This new material has good processability and high shape stability, but still suffers from the disadvantages (low latent heat storage capacity and low thermal conductivity) of traditional PCMs. In this work the PLR was selected as the support material for PEG based PCMs. Boron Nitride (BN) attracted great research interest, especially in polymer nanocomposites. As for PCMs, it has been demonstrated that the thermal conductivity has been significantly increased by adding BN in different PCMs [23], [24] and for our interest in PEG. Therefore, in this work we will try to increase the

thermal conductivity of PLR/PEG based PCM by adding BN as a filler. BN is a binary compound with a hexagonal crystalline structure and it has the capability to develop complex shapes, like 1D single-walled nanotubes or 2D single layer sheets. [25] BN can be deposited either as a single layer or as a multilayer and, depending on the fabrication process, different crystalline structures could be developed, like the cubic one with a high hardness. [26] Among their properties we can note its high thermal conductivity [27] and a high specific surface area due to its 2D structure.

Our intention in the present paper is to increase the PLR-PEG PCMs thermal conductivity with the use of BN as a filler. For this we will add different BN contents, keeping the synthesis process simple and ecofriendly, *i.e.,* only using water as solvent. Also, another goal to reach in the present paper is maintaining the excellent properties which already has PLR-PEG (such as high form stability, high flexibility and high phase transition enthalpy) in order to obtain a material with a high-performance (like the solid-solid PCM) for uses like solar energy storage, and cooling of electronic devices.

2. RESULTS AND DISCUSSION

2.1 Fabrication and structure characterization

The production of BN-doped polyrotaxane/PEG was fabricated in three steps (Figure 1a). Firstly, the polyrotaxane was synthesized following the previous work, which performed excellent shape stability [19] (See SI for specific synthesis steps). Then the previously dissolved PEG is mixed with the dissolved and previously dispersed BN, and finally mixed with the polyrotaxane. Then, through freeze-drying and hot pressing, we can obtain PCM composites with specific shape and size. It is worth pointing out that we choose 300 wt% PEG loading in this paper because it is relatively high in the late heat and maintains certain mechanical properties, especially the flexibility. As shown in **Figure 1**b-d, the sample has excellent plasticity and easily hot pressed to get designed shape. Notably, all

the samples show good flexibility (**Figure 1b, c**), which is conducive to the application in wearable devices.

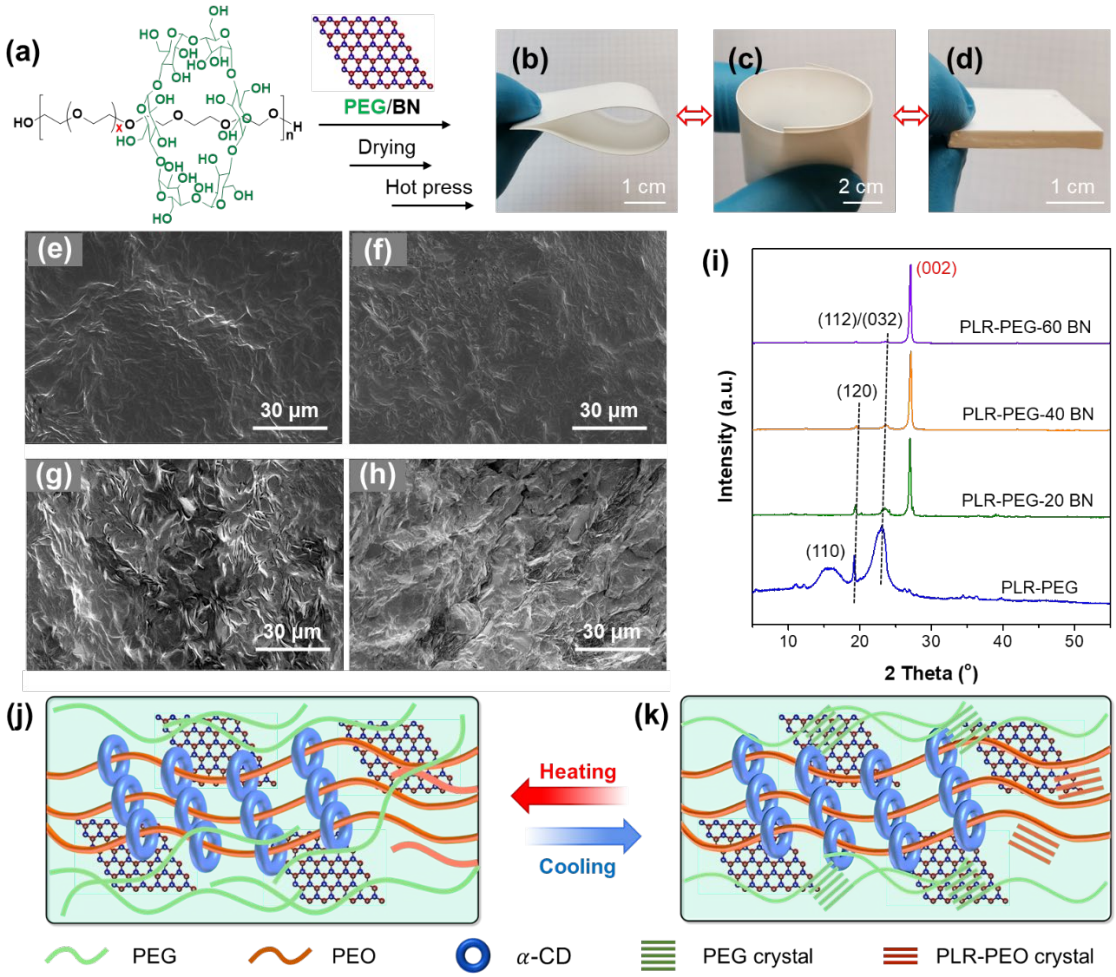

Figure 1. (a) Chemical structure of polyrotaxne and the three steps for PCM composites fabrication, (b) bent sample with size of 80 mm × 40 mm × 0.5 mm, (c) curled sample with size of 80 mm × 40 mm × 0.5 mm, (d) remolded sample with size of 40 mm × 40 mm × 4 mm. Images obtained from the SEM of the PCMs correspond to (e) PLR-PEG, (f) PLR-PEG-20 BN, (g) PLR-PEG-40 BN, (h) PLR-PEG-60 BN, (i) XRD curves of the four PCMs, (j) diagram of melting state of the PCM composites, and (k) diagram of crystalline state of the material at room temperature.

Scanning electron microscope (SEM) micrographs of fractured surface of PLR-PEG nanocomposites containing BN are illustrated in **Figure 1e-h**. As shown in Figure 1e, the

surface is relatively rough, which is because the PEG 1k assisted the movability during sample preparation. With the introduction of BN, we can see that the surface becomes rougher with a higher content of BN. It is evident that certain BN nanosheets are embedded in the PCM matrix but this nanosheets are well covered by the matrix, with no obvious gaps (Figure 1f and g) between BN nanosheets and PLR/PEG matrix, which is evidence of the good compatibility between the PCM and BN. The energy dispersive spectrometer (EDS) (Figure S1) of PLR-PEG-60BN can further proved the well dispersion of BN in the polymeric matrix.

The X-ray diffraction patterns (XRD) were shown in **Figure 1i**. We could see that all samples show two intense peaks at $2\theta \sim 19°$ and $2\theta \sim 23°$, which are attributed to crystal reflection (120) planes and concerted (112)/(032) planes of PEG, respectively, confirming the high degree of crystallinity (as calculated and listed in Table 1) of the structure. In all samples containing BN nanosheets, a very intense peak appears, which increases in intensity the higher the percentage of BN in the samples. This peak is observed at $2\theta \sim 27.1°$. This peak corresponds to the crystalline (002) plane of BN. 5.3° (001), 11.0° (002), and 12.5° (110) obtained from the PLR crystal consisting of α-Cyclodextrin and PEG. [9] Finally, the melting and solid internal molecular structure illustrations are shown in **Figure 1j** and 1k. Typically, the BN nanosheets are well dispersed in the collective, and the cyclodextrin crystal is well maintained within a certain temperature range, which acts as a physical crosslinking point and to keep the shape stability during phase transition.

Table 1. Differential Scanning Calorimeter (DSC) parameters

Samples	**$T_{m,onset}$ (ºC)**	**$T_{m,\ peak}$ (ºC)**	**$T_{s,onset}$ (ºC)**	**$T_{s,\ peak}$ (ºC)**	**ΔH_m (J/g)**	**ΔH_S (J/g)**	**Supercooling (ºC)**	**Enthlpy Efficiency%**	**Crystallinity (%)**
PLR-PEG	23.01	36.59, 57.76	34.66	31.30, 25.01	146.5	136.6	11.65	117.4	85.2

PLR-PEG-20BN	24.02	35.98, 56.54	36.28	33.55, 26.52	123.5	113.1	12.26	108.8	86.2
PLR-PEG-40BN	24.48	36.09, 56.85	36.64	34.18, 26.88	104.4	99.24	12.16	117.1	85.1
PLR-PEG-60BN	23.62	35.98, 56.79	36.77	33.93, 25.94	91.16	81.13	13.15	116.9	84.9

2.2 Phase change behaviors

As a premise of the previous work, an important property of this PCM is the shape stability [19]. We subject square samples (20 mm × 20 mm × 3 mm) to a higher temperature than PEG 1K and PLR melting temperatures [9]. In this case we will expose the samples to a temperature of 80°C for 1 h. The results can be seen in **Figure 2a**, where we can compare the photos at room temperature compared to those obtained after heat treatment. It can be clearly observed that there is not any leakage of PEG, and the sample maintains the initial shape without any obvious deformation, which directly confirmed the excellent form-stability and antileakage performances.

The heat conductivity tests in the PLR-PEG-BNs were performed using a thermal constants analyzer (TPS2500 S, Hot Disk) at room temperature with samples higher than 4 mm of thickness. The results were summarized in **Figure 2b**. The results for PLR-PEG, PLR-PEG-20 BN, PLR-PEG-40 BN, and PLR-PEG-60 BN are as follows respectively: 0.30±0.01 W/(m·K), 0.86 ±0.01 W/(m·K), 1.70 ±0.02 W/(m·K) and 2.72±0.01 W/(m·K), corresponding to an increase of 186.7%, 466.7% and 806.7%, respectively, relative to that of PLR-PEG. It is worth mentioning that high thermal conductivity is a significant property considered for the advanced thermal energy storage and heat transfer of PCMs.

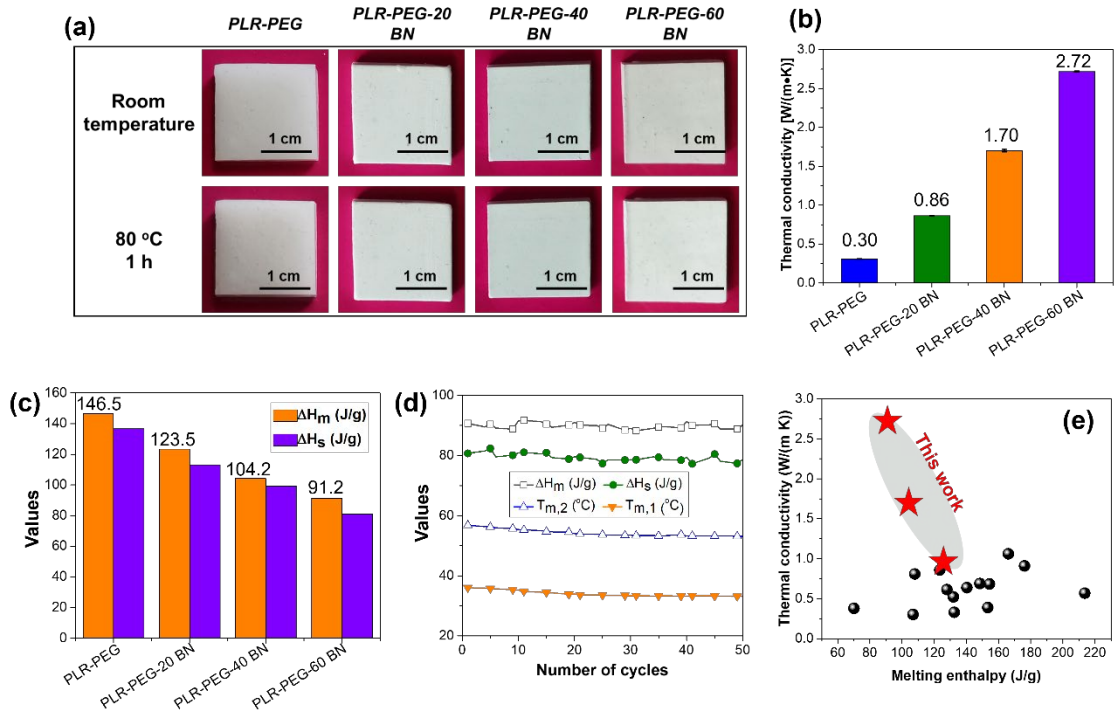

Figure 2. (a) Images of samples before and after heat treatment (80 °C, 1 h), (b) Thermal conductivity parameters of the samples, (c) Graph with data of latent heat (ΔH_m) and solidification enthalpy (ΔH_s), (d) Plots of DSC parameters of solidification enthalpy (ΔHs (J/g)) and solidification temperature T_s, latent heat (ΔH_m) and melting temperature T_m ($T_{m,2}$ for PLR and $T_{m,1}$ for PEG 1k in the PLR/PEG blend) during the 50 cycles, and (e) Comparation of ΔH_m and thermal conductivity with some typical values in recent reports elsewhere.

Table 2. Comparison with the preparation method and key parameters for the PEG-based PCMs in the recent literature elsewhere.

No.	Supporter materials	Preparation method	PCM loading rate (%)	Enthalpy efficiency (%)	Latent heat (J g^{-1})	Thermal conductivity (TC, W/(m·K))	TC enhancement (%)	References

1	Orange peel- based porous carbon	Vacuum maceration	-	88.0	140.3	0.6390	104.1	[28]
2	Silicon dioxide network with aminopropyl group and carboxylic multi-walled carbon nanotubes	Sol-gel method	84.8	-	132.5	0.3300	43.5–108.7	[29]
3	Bio-based poly (glycerol-itaconic acid)	Solvent free	-	-	70.1	0.3800	-	[30]
4	3D porous TiO_2	In situ encapsulate	92.0	-	153.3	0.3900	26.0	[31]
5	Calcium ion-crosslinked SA/kapok fiber aerogel	Vacuum impregnation	-	-	154.4	0.6840	181.5	[32]
6	Graphene oxide nanosheets modified with CoO nanoparticles	Physical mixing and melt impregnation method	80.2	99.8	131.9	0.5231	51.8-152.5	[33]
7	4’4-diphenylmethane diisocyanate	Two-step solvent	-	74.8	106.8	0.3035	1.2	[34]
8	Hydroxylated carbon nanotubes	Chemical grafting	91.0	-	127.9	0.6147	119.8	[35]
9	Graphene oxide aerogel	Vacuum impregnation	96.4	-	148.4	0.6900	181.6	[36]
10	Carbon fiber/boron nitride-based nested structure	Melt blending	63.2	59.6	107.9	0.8100	-	[37]
11	Wood flour /PLA	Melt blending	70.4	-	87.2	-	-	[38]
12	Hexamethylene diisocyanate trimer crosslinked PEG	Crosslinking	-	73.3	134.8	-	-	[39]

13	Porous framework	Vacuum impregnation	94.2-98.7	-	176.2-185.4	0.9100	387.0%	[40]
14	Carbon aerogel	Vacuum impregnation	97	-	186.6	-	-	[41]
15	Reduced graphene oxide nanosheets decorated with Ni nanoparticles nickel foam skeletons	Vacuum impregnation	-	-	125.3	0.9199	344.0	[42]
16	Scaphium scaphigerum/graphene hybrid aerogel	Vacuum impregnation	-	99.35	166.11	1.0621		[43]
17	PLR	Physical blending				2.7800	806.7%	This work

The phase change temperature and thermal energy storage properties of the PCM composites were measured by the DSC. The melting and solidifying DSC curves of the PLR-PEG BN composites are shown in **Figure S2** to **S5**.

The detailed calorimetric results of the DSC experiments are summarized in **Table 1**, including, onset solidifying temperature ($T_{s,\ onset}$), onset melting temperature ($T_{m,\ onset}$), peak melting temperature ($T_{m,\ peak}$), solidification enthalpy (ΔH_s) and melting enthalpy (ΔH_m). The melting and solidification enthalpies are reflected in **Figure 2**c and **d**. It is important to say that the melting enthalpy decreased to a certain extent (from 146.5 to 91.2 J/g). Table 1 also included values of for conventional enthalpy efficiency, extent of supercooling values and crystallinity which we have already described how to do in the materials and methods section.

As shown in **Table 1**, there are not significant difference in $T_{m,\ onset}$, $T_{m,\ peak}$, of the samples with or without BN, indicating that BN does not promote PEG crystallization

capacity. This can also be proved in the calculation results of crystallinity. The crystallinity (φ_c%) was calculated by the following equation: [44]

$$\varphi_{c,PEG+PEO}\% = \frac{\Delta H_m}{\omega_{PEG+PEO} \times \Delta H_m^0} \times 100(\%), \quad (1)$$

where ΔH_m represented the measured enthalpy of melting, ΔH_m^0 was the melting enthalpy for a 100 % crystalline material, and $\omega_{PEO+PEG}$ [%] was the fraction of the PEG and PEO in the sample. The value of ΔH_m^0 of PEO (or PEG) used in the present paper was 196.4 J g^{-1}.[45] As a result, the calculated crystallinities are 85.2%, 86.2%, 85.1%, and 84.9% for sample PLR-PEG, PLR-PEG-20 BN, PLR-PEG-40 BN and PLR-PEG-60 BN, respectively. Notably, both $T_{s,\,onset}$ and $T_{s,\,peak}$ increased to a certain extent relative to these of PLR-PEG, indicating BN can perform as a nuclear agent to prompt PEG to crystallize in advance.

For all samples, we could see the conspicuous endothermic and exothermic peak in the melting and solidification process, which represent the solid-liquid phase change. The enthalpy efficiency (E%) of PCMs (PEG) can be determined by equation (4), [46]

$$E\ \% = \frac{\Delta H_m}{\omega \times \Delta H_{PCM}} \times 100\ (\%), \quad (4)$$

where ΔH_m is the enthalpy value of the target PCMs. ΔH_{PCM} represents the enthalpy of PCM substance, namely, PEG, and ω [%] is the mass ratio of PEG in the PCMs. High values are maintained in the enthalpy efficiency, all above 100% (the calculated values are listed in Table 1), which means that it does not have much heat loss during the cooling process, indicating that latent heat can be released during the cooling stage and increase the energy efficiency.

For latent heat thermal energy storage, a cyclic stability is very important because it translates into the useful life that the PCM will have for that application. To achieve that propose, PCMs must be thermally stable over a large number of melting and cooling cycles. Therefore, we submitted one of the samples, PLR-PEG-60 BN, to have 50 DSC

cycles.

As we can see in **Figure 2**d, there is no significant change in any of the enthalpy and temperature values. This may also be due to the influence of BN due to the interaction between BN nanosheets and PEG, such as surface tension forces, and capillary forces, that will confine the mobility of PEG molecules, resulting in the decrease in phase change temperature.[47] This can occur because the BN can reinforce its function throughout the cycles ensuring stability. Based on these results it can be concluded that the PLR-PEG-60 BN composite PCM showed excellent cycling performance. Note that the detailed phase change parameters are summarized in Table S1.

Table 2 listed the PCM fabrication strategies and key parameters (such as, latent heat, PCM loading, enthalpy efficiency) from different research groups. The enthalpy and thermal conductivity of these PCMs are plotted in **Figure 2e**. As it can be seen, the properties in this work are outstanding in both enthalpy and thermal conductivity, which makes them good candidates in the thermal management of advanced devices.

2.3 Heat response

To see the thermal response and phase change behavior, we summit samples of the same size to a hot plate for heating and then cooling respectively. The IR images collected during the process can be seen in **Figure 3a**. The behavior of the PCM can be observed in the heating process: the sample is absorbing heat until it reaches the melting point with a structure collapse, then the phase change, and remains thermally stable until the phase change ends and continues absorbing heat. The mentioned phase change can be seen as a plateau in the curve (**Figure 3b**). During the cooling process is the same behavior: it goes down in temperature until it reaches its solidification temperature range. We can see the supercooling process (Figure 3c), due to the difference in melting and solidification temperatures, showing a rebound effect before entering the plateau. The curve shows that

the temperature rises at the initial stage of crystallization, which is due to the exothermic crystallization with heat release to a certain extent, which leads to the sample surface temperature increase to a certain extent.

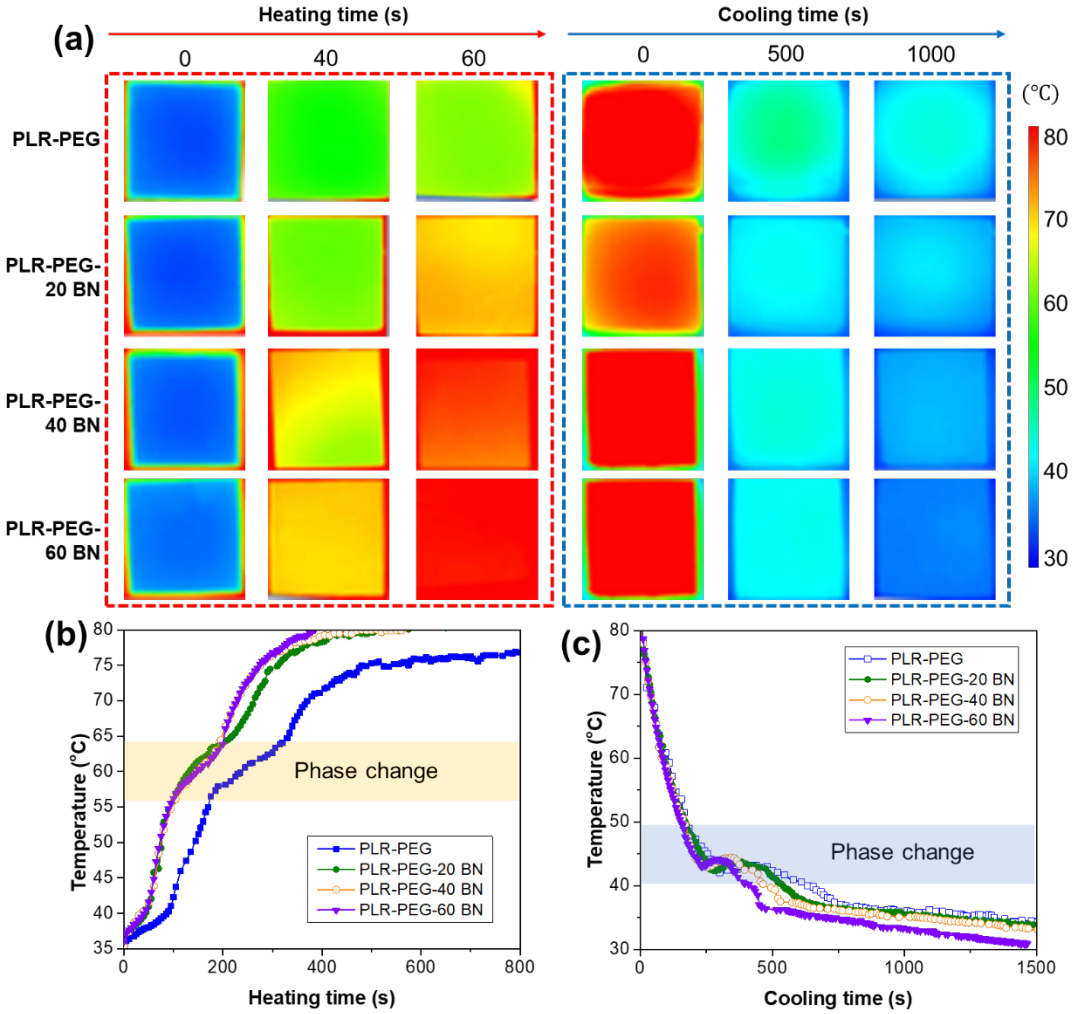

Figure 3. Heat response test: (a) Thermal images of the samples during heating and cooling process (all the samples have the same size of 20 mm × 20 mm × 3 mm), (b) the heating curves, and (c) the cooling curves of the all samples.

The phase change during the heating process occurs between 30-40 ºC for PEG 1k and 60-65 ºC for PLR and in the cooling process between 40-45 ºC. There is an evident difference in temperature increasing rate between PLR-PEG and BN-containing samples.

BN-containing samples behave with a relative fast thermal response rate of heating and cooling than the reference. This observation could confirm that the action of BN increases the thermal conductivity of the samples (Figure 2b). This property is important for some applications that require a fast heat response (meaning fast heat charge or discharge) like to thermal management of electronic devices or solar energy harvesting.

2.4 Microcalorimeter (MCC) testing and thermal stability

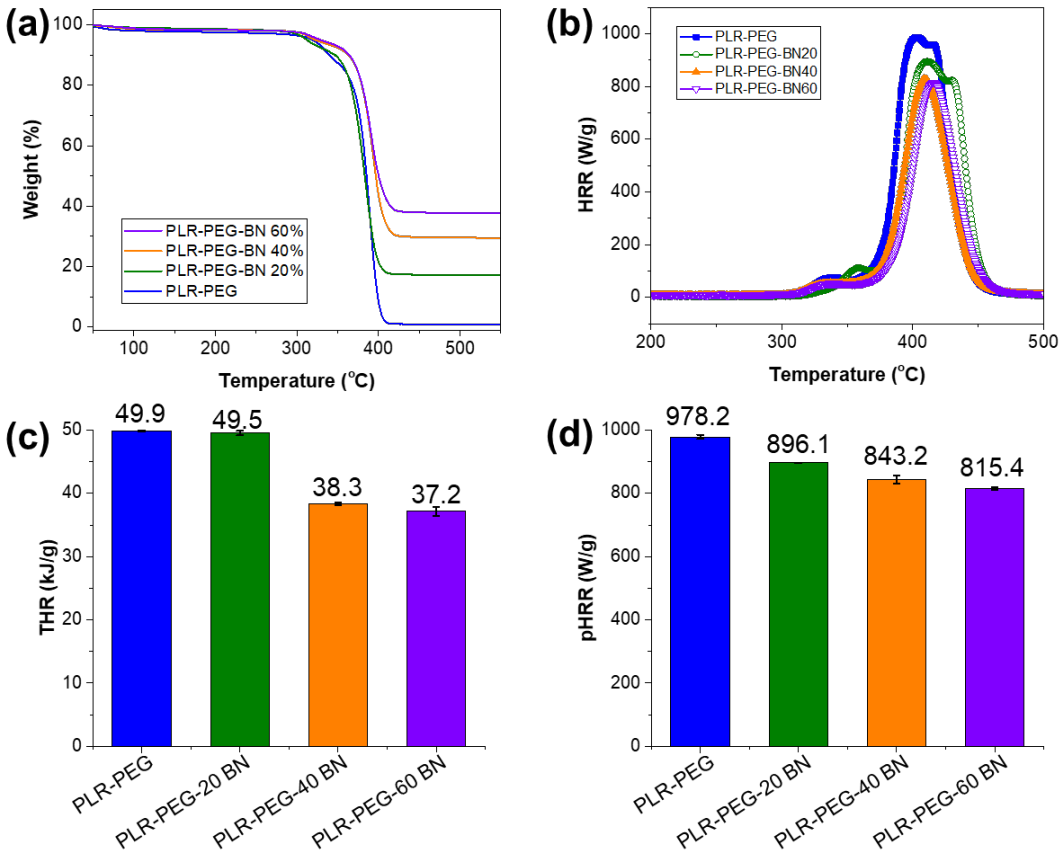

Figure 4. (a) Thermogravimetric Analysis (TGA) curves (in N_2 atmosphere), (b) Heat release rate (HRR) curves of the four samples obtained by MCC, (c) Total heat release (THR) (KJ/g) data for all the samples, and (d) Peak heat release rate (pHRR) data for all the samples.

Conversely, thermal stability is a critical parameter for the melt-processing of polymers.

The curves obtained with the TGA under N_2 atmosphere are shown in **Figure 4a** and it can be noticed that the degradation occurs in two steps, the first one corresponds to the degradation of the α-CD at ~310 °C. On the other hand, the second degradation occurs at ~380 °C and corresponds to the degradation of the PEG.[48] The residue remaining in the samples with BN, that is, the percentage of residue in accordance with the concentration of BN in the PCM, is shown in **Table 3**. All the TGA results indicated that the presence of BN does not influence the PLR-PEG thermal stability in a significant manner.

Table 3. TGA parameters and MCC results

Sample	T_{max1} (ºC)	T_{max2} (ºC)	BN content %	Residue %	pHRR (W/g)	THR (kJ/g)
PLR-PEG	336.2	389.3	-	3.08	978.2	49.9
PLR-PEG-20BN	311.2	384.2	16.67	18.00	896.1	49.5
PLR-PEG-40BN	315.1	393.5	28.57	31.18	843.2	38.3
PLR-PEG-60BN	316.0	390.9	37.50	39.30	815.4	37.2

The fire resistance in our samples was investigated using a micro combustion calorimeter (MCC). This test is used to measure the heat released by materials using small-scale oxygen consumption calorimetry, which is the main parameter for evaluation of fire resistance, quantified by the peak heat release rate (pHRR). Another important parameter is the total heat release (THR), which is the amount of heat released by the sample during whole ignition process.

As we also saw in the TGA results previously, the PCM degradation here in MCC test is done in two steps. The first peak that can be seen in **Figure 4b** belongs to the heat release due to the degradation of α-CD, while the largest peak corresponds to the

degradation of PEG and PEO. It is important to mention that all samples showed similar behavior. Thus, we could observe a HRR decrease in the two degradation peaks the higher the BN content of the sample.

As shown in **Figure 4 c-d**, we can see a slight difference between the PLR- PEG reference and the samples with a content of BN nanosheets: the decrease in both the pHRR value and the THR value can be clearly seen at larger percentages of BN (a decrease of 16.6% and 25.5%, respectively). It is worth pointing out that although BN does not show significant catalytic effect on char formation, its two-dimensional nanostructure (with its non-flammable nature and good dispersion) can act as a barrier for heat and mass conduction, thus having a positive effect on fire safety to a certain extent.

2.5 Application cases

2.5.1 Peak Shaving and Valley Filling for thermoelectric generator (TEG)

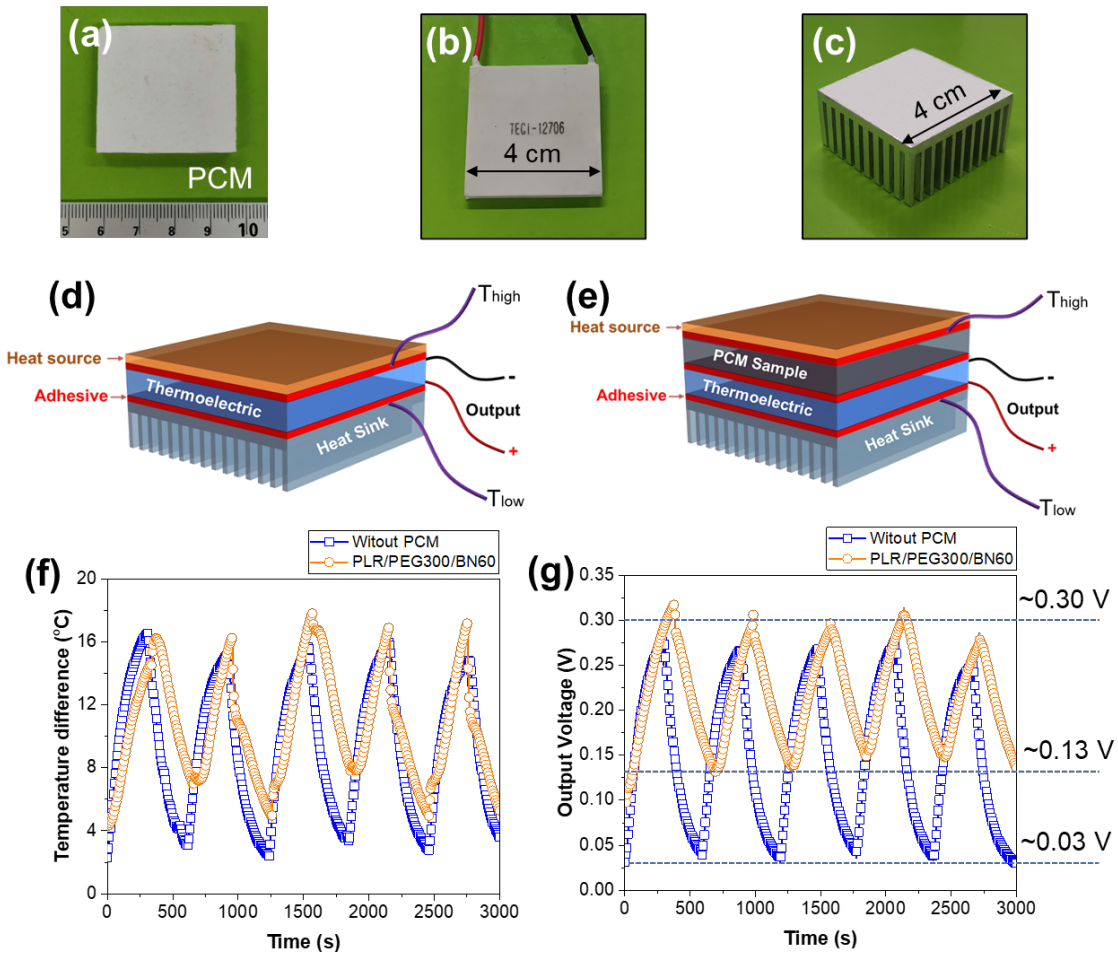

Figure 5. (a) PCM (sample PLR-PEG-60 BN) image (with size of 40 mm × 40 mm × 4 mm), (b) TEG (Model: TECI-12706), (c) Heat sink, (d) Structure illustration of the test devices without PCM, (e) Packed structure illustration of device with PCM, (f) Temperature difference of the two side of TEG (T_{high} and T_{low}), and (g) Voltage output of the two devices with or without PCM.

With the temperature and the heat absorbed by the PCM, the heat response of the generator can be delayed a little bit. Consequently, it performed as shown in the **Figure 5**f-g. Fortunately, the output voltage can be maintained at 0.13 V; however, if the sample is tested without the PCM, this voltage output will be quickly lost when the heat source is removed. An important advantage of the PCM incorporation is that the voltage output is continuous and stable. It can be seen from **Figure 5f** that the peak difference of temperature we control is almost the same. It is worth mentioning that T_{high} is the heat source temperature and T_{Low} is the temperature at the interface between heat sink and thermoelectric converter. Due to the heat storage effect during PCM heating, the temperature difference is slightly larger after cooling. Furthermore, the system containing PCM in **Figure 5g** has significantly high peak output voltage. We believe that the important reason for this phenomenon is that during the limited heating cycle the phase change of PCM will adjust the temperature difference on both sides of the thermoelectric converter. As a result, in the same heating cycle, the temperature difference is slightly higher than that of devices without PCM. Therefore, the peak value of the total voltage output is significantly lower than that of the sample without PCM. When the heat source is removed, PCM stores a certain amount of heat, which can fully serve as the heat source to maintain the temperature difference. Thus, maintaining a relatively high voltage output during cooling will play a significant practical effect of Peak Shaving and Valley Filling.

2.5.2 Smart phone thermal regulation

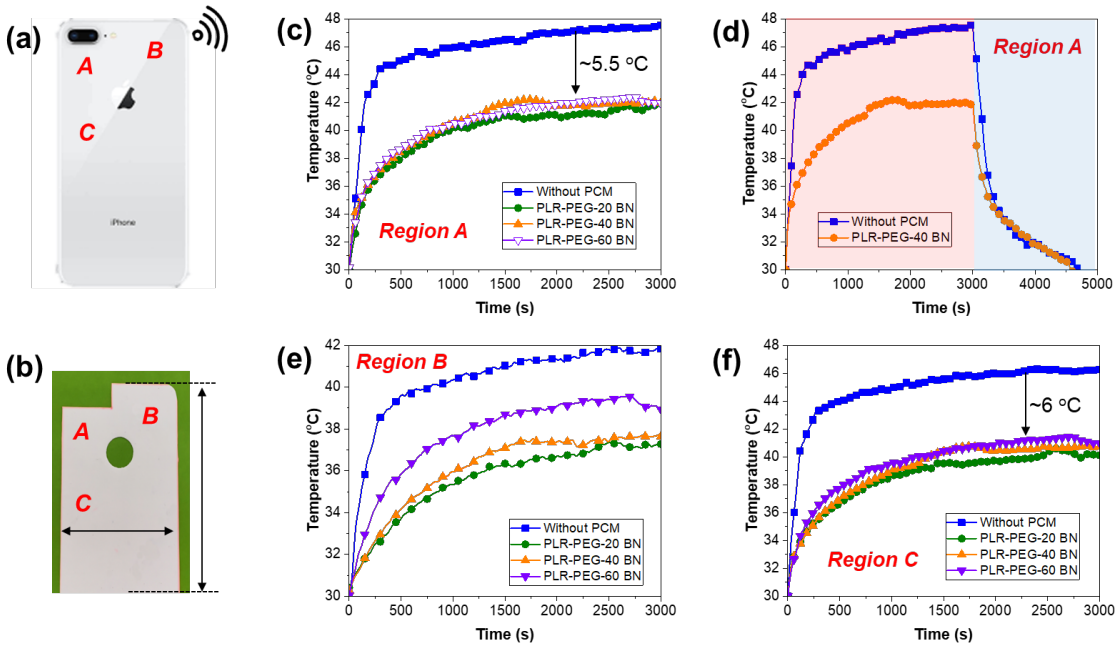

Figure 6. (a) Illustration of smart phone, (b) PCM sheet (with thickness of 0.5 mm) with designed shape according to the size of smart phone, (c) temperature increasing plots of region A (main heat source), (d) temperature increasing and decreasing of selected specimens, (e) temperature increasing plots of region B, and (f) temperature increasing plots of region C.

Figure 6a shows the image of smart phone. Figure 6b depicts the PCM composite sheet with designed shape according to the smart phone as shown in Figure 6a. We separately analyzed the temperature changes based on the region A, B and C. In general, the mobile phone system with PCM sheet has a lower temperature than that of the neat cellphone, as typically shown in Figure 6c and d. Specifically, region A (**Figure 6**c) has a temperature drop of 5.5 ^{o}C), and region C has a temperature drop of 6 ^{o}C (see **Figure 6**f). Due to the high temperature in the A and C areas, the temperature increase is mainly due to the heat absorption from cellphone. Although the sample PLR-PEG-20 BN has significantly higher latent heat of phase change than that of PLR-PEG-60 BN, the latter has a much higher thermal conductivity, so the heat is more easily diffused to the surrounding region

(such as region B), resulting that region A and C have similar trends, and have similar temperature change tendency and adjustment ability. In particular, we found that in Region B, the temperature difference of different sample systems is more obvious (see **Figure6**e). Moreover, the samples with high BN content have higher temperature at the same time. Namely, the temperature change trend is as follows: PLR-PEG-20 BN< PLR-PEG-40 BN< PLR-PEG-60 BN. Since the temperature in Region B of cellphone is relatively low, its heat source is not only the one generated by the mobile phone, but also the heat transfer from Region A and C. A combination of factors results in a sample with high thermal conductivity having a high temperature at the same time.

3. CONCLUSIONS

The PLR/PEG nanocomposites with various contents of BN nanosheets have been successfully prepared with the objective of investigating the enhanced thermal conductivity. Samples of PLR/PEG BN nanocomposites were fabricated using a blending method with water as the only solvent. The addition of BN nanosheets to PLR/PEG maintained shape stability in its phase transition. A great thermal performance is observed, obtaining high latent heat values (91.2-123.5 J/g) and cyclical stability. We can further see a significant increase in thermal conductivity between 186.7-806.7 %, compared to PLR-PEG. This increase is linear with the increase in BN content. The present research shows the improvement in fire resistance properties, lowering the values of pHRR and THR in a 16.6% and 25.5%, respectively, and heat response, obtaining faster heating and cooling rates. For the application cases, our results showed obvious Peak Shaving and Valley Filling effect and heat regulation for the smartphones. To summarize, the high thermal performance with high enthalpy values, the high thermal conductivity values, added the excellent form stability so that we obtain in PLR/PEG/ BN, allows its simple synthesis process and green pathway to make an optimal PCM to

be used as latent heat thermal energy storage material in industrial applications such as smartphone thermoregulator or thermoelectric generator.

Acknowledgment

The authors acknowledge the financial support provided by BIOFIRESAFE Project funded by Ministerio De Ciencia E Innovación (MINECO), Spain with Project number: PID2020-117274RB-I00BIOFIRESAFE.

4. REFERENCES

1. Debich B, El Hami A, Yaich A, Gafsi W, Walha LHaddar M, An efficient reliability-based design optimization study for PCM-based heat-sink used for cooling electronic devices. Mechanics of Advanced Materials and Structures 2022; 29 (12): 1661-73.
2. Kannan KGKamatchi R, Augmented heat transfer by hybrid thermosyphon assisted thermal energy storage system for electronic cooling. Journal of Energy Storage 2020; 27: 101146.
3. Sundararajan S, Samui ABKulkarni PS, Versatility of polyethylene glycol (PEG) in designing solid–solid phase change materials (PCMs) for thermal management and their application to innovative technologies. Journal of Materials Chemistry A 2017; 5 (35): 18379-96.
4. Souayfane F, Fardoun FBiwole P-H, Phase change materials (PCM) for cooling applications in buildings: A review. Energy and Buildings 2016; 129: 396-431.
5. Javadi FS, Metselaar HSCGanesan P, Performance improvement of solar thermal systems integrated with phase change materials (PCM), a review. Solar Energy 2020; 206: 330-52.
6. Gharbi S, Harmand SJabrallah SB, Experimental comparison between different configurations of PCM based heat sinks for cooling electronic components. Applied Thermal Engineering 2015; 87: 454-62.
7. Sarier NOnder E, Organic phase change materials and their textile applications: An overview. Thermochimica Acta 2012; 540: 7-60.
8. Aftab W, Huang X, Wu W, Liang Z, Mahmood AZou R, Nanoconfined phase change materials for thermal energy applications. Energy & Environmental Science 2018; 11 (6): 1392-424.
9. Yin G-Z, Hobson J, Duan YWang D-Y, Polyrotaxane: New generation of sustainable, ultra-flexible, form-stable and smart phase change materials. Energy Storage Materials 2021; 40: 347-57.
10. Chen R, Yao R, Xia WZou R, Electro/photo to heat conversion system based on polyurethane embedded graphite foam. Applied Energy 2015; 152: 183-8.
11. Yuan P, Zhang P, Liang TZhai S, Effects of surface functionalization on thermal and mechanical properties of graphene/polyethylene glycol composite phase change materials. Applied Surface Science 2019; 485: 402-12.
12. Jiang Y, Wang Z, Shang M, Zhang ZZhang S, Heat collection and supply of interconnected netlike graphene/polyethyleneglycol composites for thermoelectric devices. Nanoscale 2015; 7 (25): 10950-3.

13. Sundararajan S, Samui ABKulkarni PS, Interpenetrating phase change polymer networks based on crosslinked polyethylene glycol and poly(hydroxyethyl methacrylate). Solar Energy Materials and Solar Cells 2016; 149: 266-74.
14. Sarier NOnder E, The manufacture of microencapsulated phase change materials suitable for the design of thermally enhanced fabrics. Thermochimica Acta 2007; 452 (2): 149-60.
15. Ding E-Y, Jiang YLi G-K, COMPARATIVE STUDIES OF THE STRUCTURES AND TRANSITION CHARACTERISTICS OF CELLULOSE DIACETATE MODIFIED WITH POLYETHYLENE GLYCOL PREPARED BY CHEMICAL BONDING AND PHYSICAL BLENDING METHODS*. Journal of Macromolecular Science, Part B 2001; 40 (6): 1053-68.
16. Şentürk SB, Kahraman D, Alkan CGökçe İ, Biodegradable PEG/cellulose, PEG/agarose and PEG/chitosan blends as shape stabilized phase change materials for latent heat energy storage. Carbohydrate Polymers 2011; 84 (1): 141-4.
17. Wei X, Jin X-z, Zhang N, Qi X-d, Yang J-h, Zhou Z-w, Wang Y, Constructing cellulose nanocrystal/graphene nanoplatelet networks in phase change materials toward intelligent thermal management. Carbohydrate Polymers 2021; 253: 117290.
18. Yang J, Qi G-Q, Liu Y, Bao R-Y, Liu Z-Y, Yang W, Xie B-H, Yang M-B, Hybrid graphene aerogels/phase change material composites: Thermal conductivity, shape-stabilization and light-to-thermal energy storage. Carbon 2016; 100: 693-702.
19. Fan X, Liu L, Jin X, Wang W, Zhang STang B, MXene Ti3C2Tx for phase change composite with superior photothermal storage capability. Journal of Materials Chemistry A 2019; 7 (23): 14319-27.
20. Xue F, Jin X-z, Xie X, Qi X-d, Yang J-hWang Y, Constructing reduced graphene oxide/boron nitride frameworks in melamine foam towards synthesizing phase change materials applied in thermal management of microelectronic devices. Nanoscale 2019; 11 (40): 18691-701.
21. Chen X, Gao H, Yang M, Dong W, Huang X, Li A, Dong C, Wang G, Highly graphitized 3D network carbon for shape-stabilized composite PCMs with superior thermal energy harvesting. Nano Energy 2018; 49: 86-94.
22. Shi J, Qin M, Aftab WZou R, Flexible phase change materials for thermal energy storage. Energy Storage Materials 2021; 41: 321-42.
23. Silakhori M, Fauzi H, Mahmoudian MR, Metselaar HSC, Mahlia TMIKhanlou HM, Preparation and thermal properties of form-stable phase change materials composed of palmitic acid/polypyrrole/graphene nanoplatelets. Energy and Buildings 2015; 99: 189-95.
24. Yavari F, Fard HR, Pashayi K, Rafiee MA, Zamiri A, Yu Z, Ozisik R, Borca-Tasciuc T, Koratkar N, Enhanced Thermal Conductivity in a Nanostructured Phase Change Composite due to Low Concentration Graphene Additives. The Journal of Physical Chemistry C 2011; 115 (17): 8753-8.
25. Jiang X-F, Weng Q, Wang X-B, Li X, Zhang J, Golberg D, Bando Y, Recent Progress on Fabrications and Applications of Boron Nitride Nanomaterials: A Review. Journal of Materials Science & Technology 2015; 31 (6): 589-98.
26. Djouadi MA, Mortet V, Khandozhko S, Jouan PYNouet G, Dynamic stress investigations for cubic boron nitride films deposited by triode sputtering technique. Surface and Coatings Technology 2001; 142-144: 899-905.
27. Belkerk BE, Achour A, Zhang D, Sahli S, Djouadi MAYap YK, Thermal conductivity of vertically aligned boron nitride nanotubes. Applied Physics Express 2016; 9 (7): 075002.
28. Xiao S, Zou M, Xie Y, Chen W, Hu X, Ma Y, Zu S, Che Y, Jiang X, Nanosilver modified navel orange peel foam/polyethylene glycol composite phase change materials with improved thermal conductivity and photo-thermal conversion efficiency. Journal of Energy Storage 2022; 56: 105976.
29. Yan D, Ming W, Liu S, Yin G, Zhang Y, Tang B, Zhang S, Polyethylene glycol (PEG)/silicon dioxide grafted aminopropyl group and carboxylic multi-walled carbon nanotubes (SAM) composite as phase change material for light-to-heat energy conversion and storage. Journal of Energy Storage 2021; 36: 102428.

30. Yin G-Z, Yang X-M, Hobson J, López AMWang D-Y, Bio-based poly (glycerol-itaconic acid)/PEG/APP as form stable and flame-retardant phase change materials. Composites Communications 2022; 30: 101057.
31. Sun X, Yi M, Feng B, Liu R, Sun L, Zhai L, Cao H, Zou C, Shape-stabilized composite phase change material PEG@TiO2 through in situ encapsulation of PEG into 3D nanoporous TiO2 for thermal energy storage. Renewable Energy 2021; 170: 27-37.
32. Zhang Q, Chen B, Wu K, Nan B, Lu MLu M, PEG-filled kapok fiber/sodium alginate aerogel loaded phase change composite material with high thermal conductivity and excellent shape stability. Composites Part A: Applied Science and Manufacturing 2021; 143: 106279.
33. Li Y, Li Y, Huang X, Zheng H, Lu G, Xi Z, Wang G, Graphene-CoO/PEG composite phase change materials with enhanced solar-to-thermal energy conversion and storage capacity. Composites Science and Technology 2020; 195: 108197.
34. Gao N, Tang T, Xiang H, Zhang W, Li Y, Yang C, Xia T, Liu X, Preparation and structure-properties of crosslinking organic montmorillonite/polyurethane as solid-solid phase change materials for thermal energy storage. Solar Energy Materials and Solar Cells 2022; 244: 111831.
35. Yang Y, Yin Q, Xu F, Sun L, Xia Y, Guan Y, Liao L, Zhou T, Lao J, Wang Y, Wang Y, Song L, Li D, Fabricated Polyethylene glycol/ hydroxylated carbon nanotubes shape-stabilized phase change materials with improving thermal conductivity. Thermochimica Acta 2022; 718: 179363.
36. Bao Z, Bing N, Yao H-R, Zhang Y, Xie HYu W, Three-Dimensional Interpenetrating Network Phase-Change Composites with High Photothermal Conversion and Rapid Heat Storage and Release. ACS Applied Energy Materials 2021; 4 (8): 7710-20.
37. Gong S, Li X, Sheng M, Liu S, Zheng Y, Wu H, Lu X, Qu J, High Thermal Conductivity and Mechanical Strength Phase Change Composite with Double Supporting Skeletons for Industrial Waste Heat Recovery. ACS Applied Materials & Interfaces 2021; 13 (39): 47174-84.
38. Sheng M, Sheng Y, Wu H, Liu Z, Li Y, Xiao Y, Lu X, Qu J, Bio-based poly (lactic acid) shaped wood-plastic phase change composites for thermal energy storage featuring favorable reprocessability and mechanical properties. Solar Energy Materials and Solar Cells 2023; 252: 112186.
39. Fang Y, Li Z, Li X, Wu H, Sheng M, Lu X, Qu J, A novel covalent polymerized phase change composite with integrated shape memory, self-healing, electromagnetic shielding and multi-drive thermal management functions. Chemical Engineering Journal 2023; 459: 141600.
40. Liu Z, He F, Li Y, Jiang Z, He G, Lin C, Zhang Q, Zhou Y, Yang W, Enhanced solar/electric-to-thermal energy conversion capability of double skeleton based shape-stabilized phase change materials. Solar Energy Materials and Solar Cells 2023; 252: 112171.
41. Lin F, Liu X, Leng G, Bai Y, Feng J, Guo Z, Wang Z, Huang Z, Mi R, Min X, Hu X, Grid structure phase change composites with effective solar/electro-thermal conversion for multi-functional thermal application. Carbon 2023; 201: 1001-10.
42. Yang R, Huang X, Zhao G, Liu ZWang G, Ni@rGO into nickel foam for composite polyethylene glycol and erythritol phase change materials. Chemical Engineering Journal 2023; 451: 138900.
43. Wang KWen R, Scaphium scaphigerum/graphene hybrid aerogel for composite phase change material with high phase change enthalpy and high thermal conductivity for energy storage. Journal of Energy Storage 2023; 58: 106302.
44. Yin G, Zhao D, Wang X, Ren Y, Zhang L, Wu X, Nie S, Li Q, Bio-compatible poly(ester-urethane)s based on PEG-PCL-PLLA copolymer with tunable crystallization and bio-degradation properties. RSC Advances 2015; 5 (96): 79070-80.
45. Chrissopoulou K, Andrikopoulos KS, Fotiadou S, Bollas S, Karageorgaki C, Christofilos D, Voyiatzis GA, Anastasiadis SH, Crystallinity and Chain Conformation in PEO/Layered Silicate Nanocomposites. Macromolecules 2011; 44 (24): 9710-22.
46. Cheng P, Gao H, Chen X, Chen Y, Han M, Xing L, Liu P, Wang G, Flexible monolithic phase change material based on carbon nanotubes/chitosan/poly(vinyl alcohol). Chemical Engineering Journal 2020; 397: 125330.

47. He L, Wang H, Zhu H, Gu Y, Li XMao X, Thermal Properties of PEG/Graphene Nanoplatelets (GNPs) Composite Phase Change Materials with Enhanced Thermal Conductivity and Photo-Thermal Performance. Applied Sciences 2018; 8 (12): 2613.
48. Yin G-Z, Zhou M-H, García MFARincón Arévalo P, Surface grafting POSS to improve the hydrophobicity and fire safety of Polyrotaxane based smart phase change materials. Advanced Industrial and Engineering Polymer Research 2023: